ARTICLE NO. 79-1647R

Maximum Side Forces and Associated Yawing Moments on Slender Bodies

J. Peter Reding* and Lars E. Ericsson†
Lockheed Missiles & Space Co., Inc., Sunnyvale, Calif.

A method is presented for determining the maximum vortex-induced side force and associated yawing moment on slender bodies at high angles of attack in incompressible flow at effective crossflow Reynolds numbers from 10^4 to 10^8. An analogy with two-dimensional unsteady flow separation on a cylinder normal to the flow is used to bound the maximum steady vortex-induced side force on slender bodies of revolution. It is shown that the maximum vortex-induced side force occurs in the critical effective Reynolds number range when subcritical separation occurs on one side of the body and supercritical separation on the other. Although the method applies only to bodies dominated by a single asymmetric vortex pair, it could be extended to provide a basic building block for bounding the directional stability of long bodies affected by multiple asymmetric vortex pairs.

Nomenclature

$C_{m\alpha}$ = $\partial C_m/\partial\alpha$
$C_{N\alpha}$ = $\partial C_N/\partial\alpha$
c = reference length ($c=d$)
d = maximum diameter for body of revolution
$\bar{d}$ = mean diameter $= 2\int_0^l r\,\mathrm{d}\left(\frac{x}{l}\right)$
d' = sectional drag: coefficient $c_d = d'/(\rho_\infty U_\infty^2/2)c$
d_x = crossflow drag: coefficient $c_{dx} = d_x/(\rho_\infty^2/2)c$
l = sectional lift: coefficient $c_l = l/(\rho_\infty U_\infty^2/2)c$
M_∞ = freestream Mach number
m = pitching moment: coefficient $C_m = m/(\rho_\infty U_\infty^2/2)Sc$
n = yawing moment: coefficient $C_n = n/(\rho_\infty U_\infty^2/2)Sc$
N = normal force: coefficient $C_N = N/(\rho_\infty U_\infty^2/2)S$
p = static pressure: coefficient $C_p = (p-p_\infty)/(\rho_\infty U_\infty^2/2)$
r = local radius of body of revolution
R, R_d = Reynolds number $= U_\infty d/v_\infty$
S = reference area $= \pi c^2/4$
U_∞ = freestream velocity
Y = side force: coefficient $C_Y = Y/(\rho_\infty U_\infty^2/2)S$
α = angle of attack
β = sideslip angle
v_∞ = freestream kinematic viscosity
ρ_∞ = freestream air density
Φ = roll angle
σ = surface upwash angle

Subscripts

CP = center of pressure
eff = effective
max = maximum
p or peak = peak amplitude
rms = root mean square value
v = vortex induced
wet = wetted length

Superscripts

$\bar{[\ ]}$ = integrated mean parameter value
$(\bar{[\ ]}^2)^{1/2}$ = root mean square value

Presented as Paper 79-1647 at the AIAA Atmospheric Flight Mechanics Conference, Boulder, Colo., Aug. 6-8, 1979; submitted Oct. 23, 1979; revision received March 27, 1980. Copyright © 1980 by J.P. Reding. Published by the American Institute of Aeronautics and Astronautics with permission.

Index categories: LV/M Aerodynamics; Subsonic Flow; Jets, Wakes, and Viscid-Inviscid Flow Interactions.

*Staff Engineer. Associate Fellow AIAA.
†Senior Consulting Engineer. Associate Fellow AIAA.

Introduction

It has long been recognized that large side forces occur on slender bodies at high angles of attack and zero sideslip due to vortex asymmetry.[1] Current high angle of attack requirements for missiles and aircraft have resulted in renewed interest in this problem. Experimental results have shown that the vortex-induced side force can in certain cases exceed the normal force.[2] The vortex-induced side force is extremely sensitive to Reynolds number and Mach number[3,4] as well as to small surface irregularities which not only affect the magnitude of the side force but also determine its direction, left or right.[4,5]

Ever since the original work by Thomson and Morrison,[6] most theoretical techniques have used the principle of space-time equivalence to relate the steady three-dimensional vortex array to the unsteady two-dimensional vortex street. These techniques, as well as more recent ones which use numerical methods, rely upon experimental results to specify certain constants used in the theory. Because the experiments normally are conducted on subscale models, the theory does not necessarily apply to the Reynolds number range of practical interest. Furthermore, unless the experimentor has searched for the maximum vortex-induced side force by carefully varying angle of attack, roll angle, and Mach number, the theory will not predict the maximum vortex-induced side force possible even at the subscale Reynolds number. It is crucial that the missile or aircraft designer knows that the control system can cope with the maximum side force the vehicle can experience in flight. Therefore, an engineering method of determining the maximum possible vortex-induced side force has been suggested[7] for use by the designer until an adequate theoretical technique can be developed. The method relates the steady three-dimensional vortex asymmetry to the instantaneous, unsteady, two-dimensional vortex asymmetry on a cylinder normal to the flow through the use of an ef-

fective crossflow Reynolds number. The present paper improves this technique through a better definition of the peak, unsteady, two-dimensional cylinder loads and extends it to provide prediction of the accompanying yawing moment.

The Effective Reynolds Number

There is experimental evidence that the maximum side force on slender bodies at high α occurs in the Reynolds number range (based on body diameter) where the two-dimensional crossflow switches from laminar to turbulent.[7] This is true of the data of Nelson and Fleeman[8] and Keener et al.[9] Thus, it was postulated that in this critical Reynolds number range asymmetric transition could occur resulting in subcritical (laminar) separation on one side of the body and supercritical (turbulent) separation on the other. Recent unpublished pressure data[10,11] demonstrate that this subcritical-supercritical separation geometry does indeed occur on slender bodies at high angles of attack. The pressure distributions on a slender body, normalized to the normal component of the dynamic pressure, are compared in Fig. 1 to two-dimensional pressure distributions from Hoerner.[12] At $x/d=6.1$, the pressures on opposite sides of the slender body are in good agreement with the two-dimensional subcritical and supercritical pressure distributions, respectively. Secondary peaks occur in the pressure distributions over the slender body at $\varphi=55$ and 305 deg, respectively, generated by asymmetric vortices. At $x/d=8.75$, these secondary peaks merge with the suction peaks just upstream of separation. There is also an undershoot of the two-dimensional, subcritical, suction pressures at $x/d=8.75$.

To affect separation, transition must occur upstream of the lateral meridian in the crossflow plane. Atraghji's oil flow photographs[13] show that the crossflow streamlines that feed separation are elevated above the freestream through an angle $(\sigma-\alpha)$ due to acceleration of the crossflow around the body (Fig. 2). Aside from the initial transient, the feeding streamlines are contained in the intersection between the cylinder and a plane inclined at an angle σ relative to the cylinder axis. For incompressible flow potential theory gives $\sigma=\tan^{-1}(2\tan\alpha)$.

The condition of the boundary layer at separation is determined by the viscous flow following the elliptical path around the body from the windward to the lateral meridian in the σ-plane. Thus, it is this wetted length that determines the critical Reynolds number for slender bodies at high α. For $\alpha>30$ deg, the ellipse has an axis ratio less than 2 and the wetted length can be approximated as follows:

$$l_{\text{wet}}=(\pi d/8)\,(1+\operatorname{cosec}\sigma) \tag{1}$$

The corresponding Reynolds number is $R_{\text{wet}}=U_\infty\cos(\sigma-\alpha)l_{\text{wet}}/v_\infty$, i.e.,

$$R_{\text{wet}}=\frac{\pi}{8}\left(\frac{U_\infty d}{v_\infty}\right)\left\{\frac{\cos\alpha\cot\alpha+2\sin\alpha}{2}\right\}\left\{\frac{1+[1+\tfrac{1}{2}\cot\alpha)^2]^{1/2}}{[1+(\tfrac{1}{2}\cot\alpha)^2]^{1/2}}\right\} \tag{2}$$

and the effect of flow inclination on the Reynolds number at the separation point is

$$\left[\frac{R(\alpha)}{R(90^\circ)}\right]_{\text{wet}}=\left\{\frac{\cos\alpha\cot\alpha+2\sin\alpha}{2}\right\}\left\{\frac{1+[1+(\tfrac{1}{2}\cot\alpha)^2]^{1/2}}{[1+(\tfrac{1}{2}\cot\alpha)^2]^{1/2}}\right\} \tag{3}$$

Equation (3) can be used to relate the effective Reynolds number to the Reynolds number based on freestream conditions, R_{eff}/R_d, for $\alpha<30$ deg where crossflow dominates transition (Fig. 3). However, when $\alpha<30$ deg, the axial flow can have an important effect on transition[14] and this relationship no longer holds. Thus, where the simplified two-dimensional analogy in Fig. 2 applies (i.e., for $\alpha\geq 30$ deg) one can, according to Fig. 3, use the following approximation without causing more than 10% error:

$$R_{\text{eff}}\approx R_d \tag{4}$$

This explains the good correlation between the maximum side force on slender bodies at high α and the critical Reynolds number (R_d) for a cylinder normal to the flow.

That this effective Reynolds number does describe the viscous effects on slender bodies at high angle of attack is shown by the superior collapse of the Bursnall-Loftin data[15] in the critical Reynolds number region.[16] The same conclusion has been reached by Clark[17] who tried to correlate his crossflow drag using the different analytic models available:

1) The standard approach based on the normal component of velocity, i.e., $R_{\text{eff}}=R_d\sin\alpha$ (Fig. 4a);

2) The model suggested by Lamont and Hunt,[18] i.e., $R_{\text{eff}}=R_d/\sin\alpha$ (Fig. 4b);

3) A simplified form of the present model based on the small angle approximation $\sigma=2\alpha$, i.e., $R_{\text{eff}}=R_d/\sin 2\alpha$ (Fig. 4c); and finally

4) The present method which is clearly superior to all the others (Fig. 4d). It should be pointed out that for bodies with changing cross sections an effective diameter, $\bar{d}$, is used where

$$\bar{d}=2\int_0^l r\,\mathrm{d}\left(\frac{x}{l}\right) \tag{5}$$

Maximum Vortex-Induced Side Force

It is assumed that the maximum vortex-induced side force on the slender body is bounded by the peak unsteady lift occurring on a cylinder normal to the flow. The pressure distributions in Fig. 1 show that the pressures on an inclined slender body can overshoot the steady two-dimensional values substantially; however, they cannot overshoot the peak unsteady two-dimensional values. This is, of course, in full accord with the impulsively started cylinder analogy.[19] Very large dynamic overshoots of static loads have been recorded in the case of dynamic stall of airfoils.[20-22] Thus, the peak unsteady lift on a two-dimensional cylinder represents the upper bound for the maximum steady out-of-plane force (the side force), in the three-dimensional case of an inclined slender body. The normalizing in-plane forces for the two cases are the steady drag and the normal force respectively. Thus, the maximum sectional side force to normal force ratio for the inclined slender body is bounded by the ratio of the peak unsteady lift to steady drag ratio on a cylinder in two-dimensional flow

$$\frac{\mathrm{d}\,|C_Y|_{\max}}{\mathrm{d}x}\Big/\frac{\mathrm{d}C_N}{\mathrm{d}x}=\frac{c_{l_p}}{(\overline{c_l^2})^{1/2}}\frac{(\overline{c_l^2})^{1/2}}{c_d}=\frac{c_{l_p}}{c_d} \tag{6}$$

The normalization of the maximum side force with the normal force facilitates the estimation of the maximum side force for a variety of body lengths and angles of attack. One need only estimate the normal force for the particular body and angle of attack of interest, using a technique that accounts for the vortex-induced additional lift (e.g., Allen and Perkins[23] or Jorgensen[24]), and multiply it by the c_{l_p}/c_d value for the correct effective Reynolds number.‡ Thus, experimental trends such as the decrease in $|C_Y|$ with decreasing l_N/d are automatically accounted for since C_N decreases as l_N/d decreases. This technique is valid only for

‡From Eq. (4) $R_{\text{eff}}=R_d$ for a cylindrical body while for an area changing configuration $R_{\text{eff}}=R_d(\bar{d}/d)$.

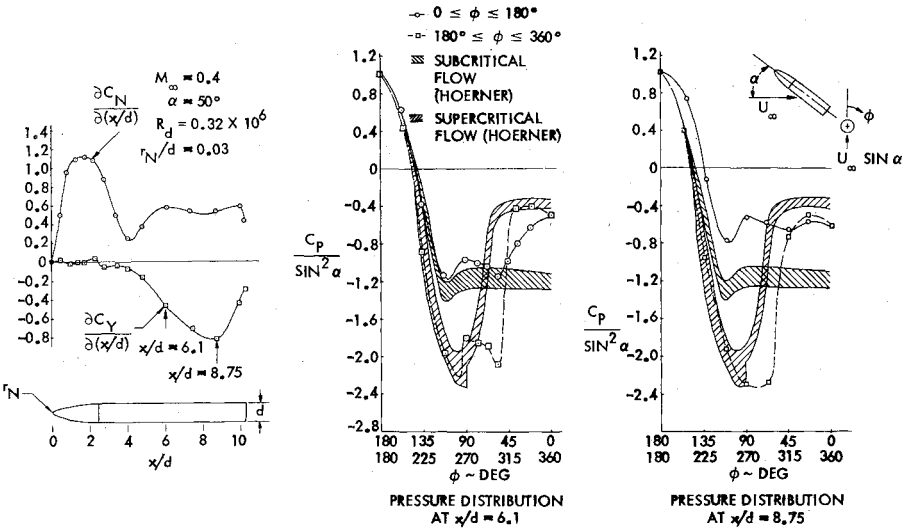

Fig. 1 Evidence of supercritical-subcritical separation on slender body at critical Reynolds number.[10]

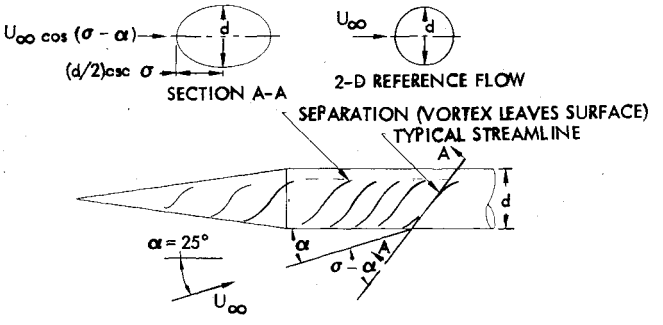

Fig. 2 Typical high-α streamlines.

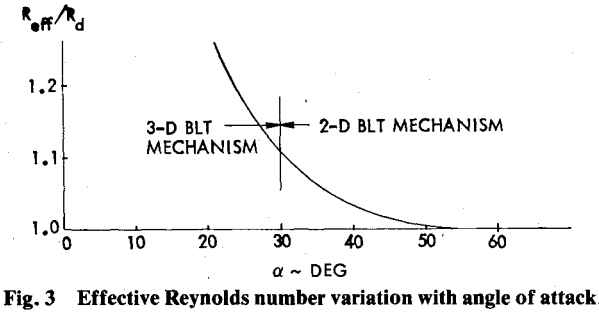

Fig. 3 Effective Reynolds number variation with angle of attack.

bodies dominated by a single vortex pair. Multiple vortex pairs result in cells of asymmetric vortices along the body which produce alternating side force components.

To determine the maximum c_{l_p}/c_d as a function of Reynolds number, an extensive literature search was conducted for unsteady two-dimensional cylinder lift data. The lift measurements were usually presented as root-mean-square (rms) sectional lift values, $(\overline{c_l^2})^{1/2}$. These data[25-38] are presented in Fig. 5. It can be seen that there is considerable data scatter. A further difficulty is the determination of the critical Reynolds number. Wind tunnel turbulence and model roughness exert a dominating influence over the critical Reynolds number causing a considerable spread for a variety of tests. Humphreys has attempted to determine the critical Reynolds number bounds due to these effects.[26] These bounds are presented in Fig. 5 for both $(\overline{c_l^2})^{1/2}$ and c_d.

Humphreys measured both the peak and the rms fluctuating lift at subcritical Reynolds numbers.[26] Fung made similar measurements at supercritical Reynolds numbers.[27] These are the only peak lift measurements known to the authors and have, therefore, been used to determine the ratio, $c_{l_p}/(\overline{c_l^2})^{1/2}$ (Fig. 6). The data have been shifted to agree with the critical Reynolds number limits of Fig. 5 and together with the data in Fig. 5 they define the peak lift c_{l_p} curve. This c_{l_p} curve, when divided by Jorgensen's drag data[24] (shifted to agree with the critical Reynolds number bounds in Fig. 5), defines the bounds of the peak two-dimensional sectional lift/drag ratio (c_{l_p}/c_d), which should bound the maximum sectional side force/normal force ratio $(d|C_Y|_{max}/dx)/(dC_N/dx)$ for the inclined slender body.§ Figure 7 demonstrates that this curve does bound all the sectional data available to the authors. Moreover, the good agreement with Bearman's measured lift peak for a cylinder normal to the flow[39] verifies the very large c_{l_p}/c_d level at critical Reynolds numbers. Bearman's flow visualization results indicated that the stationary subcritical-supercritical separation geometry had resulted from the collapse of the laminar separation bubble on one side of the cylinder. Thus, this data point does indeed represent the true maximum c_{l_p}/c_d value which bounds the sectional $(d|C_Y|_{max}/dx)/(dC_N/dx)$.¶

The pressure data on the inclined slender body[10] showed the vortex-induced normal force distribution on the cylinder to be more or less rectangular whereas the side force distribution was roughly triangular (Fig. 1). These results are typical. Thus, the overall vortex-induced side force to normal force ratio for a single asymmetric vortex pair (a cell) is:

$$|C_Y|_{max}/C_N = \tfrac{1}{2}c_{l_p}/c_d \qquad (7)$$

This boundary encloses all experimental $|C_Y|_{max}/C_N$ data known to the authors for $\alpha > 30$ deg, (i.e., where the two-dimensional analogy is valid)[1,2,4,9,13,41-43] (Fig. 8). This includes a large body of data where the maximum side force has been defined through a 360-degree variation of the roll angle.[2,4,9,42]

The limiting $|C_Y|_{max}/C_N$ values are realized only when one asymmetric vortex pair exists over the entire length of the body. This occurs on low fineness ratio pointed bodies (ogives, cones, etc.) where the vortex asymmetry begins to develop immediately near the apex. This explains why the data for $l/d = 3.5$ and 5.0 ogives and for 8- and 10-deg cones

§Jorgensen's drag data[24] are presented in Fig. 5 as measured and are also shifted to agree with Humphrey's critical Reynolds number limits.

¶To define the upper bound of the vortex-induced side-force/normal force ratio, one must use incompressible data because vortex-induced loads tend to diminish with increasing Mach number.[40]

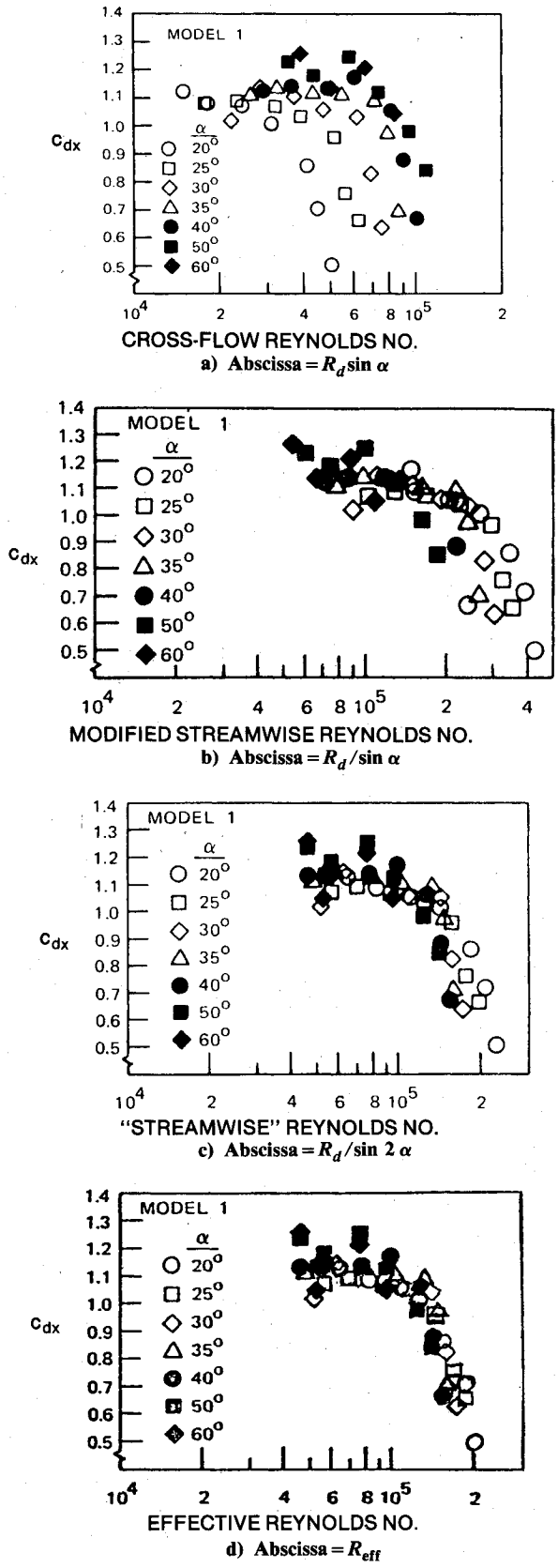

Fig. 4 Crossflow drag correlation with Reynolds number defined in various manners.

fall close to the upper boundary in Fig. 8. This $|C_Y|_{max}/C_N$ curve is to be used to predict the maximum vortex-induced side force at $30° \leq \alpha \leq 70°$ and $10^4 \leq R_{eff} \leq 10^8$. (This limit will only be approached at incompressible crossflow Mach numbers.)

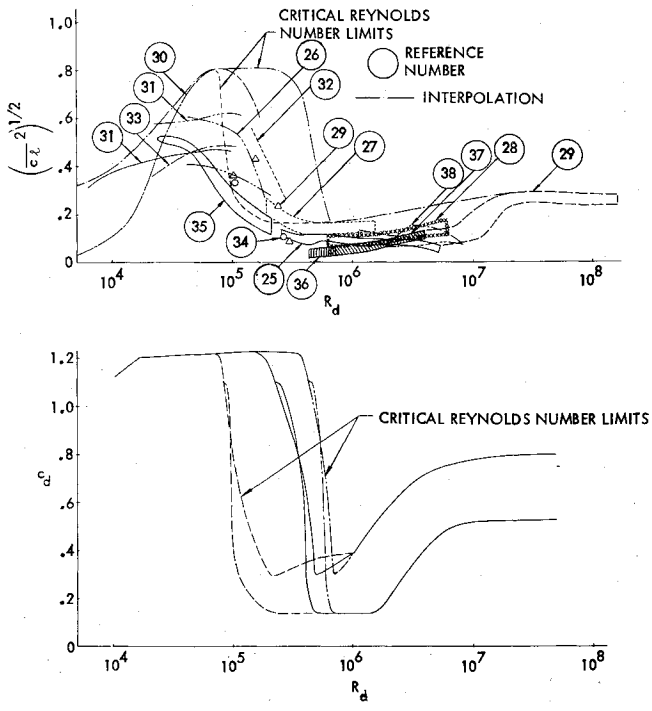

Fig. 5 Correlation of root-mean-square lift with steady drag for a cylinder in crossflow.

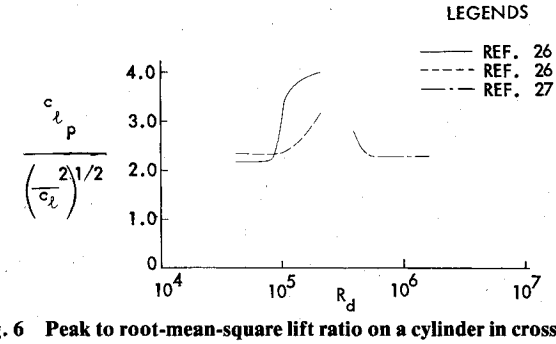

Fig. 6 Peak to root-mean-square lift ratio on a cylinder in crossflow.

Maximum Vortex-Induced Yawing Moment

Knowing the maximum vortex-induced side force is not enough for control system design or stability analysis. One must also know where the side force acts. For relatively low fineness ratio pointed bodies dominated by a single asymmetric vortex pair, or for aircraft, where the concern is the vortex-induced side force generated on the pointed nose at high angles of attack, one is interested in knowing the center of pressure of the maximum side force induced by a single vortex pair. For longer bodies this will also be the case of greatest concern if the nose is slender and pointed. Even in the case where multiple, alternating, asymmetric vortex cells exist along the body, a technique that bounds the yawing moment contribution from the single cell can provide a basic building block for a more generally applicable method.

The pressure data discussed earlier[10] (Fig. 1) showed the vortex-induced side force on a cylinder to have a triangular distribution, while the normal force distribution was rectangular. Using these distributions as unit area weighing functions, the centers of pressure for normal force and side force on an $l/d = 3.5$ pointed ogive were computed. Experimental data[10] indicate that the maximum side force is obtained with one pair of asymmetric vortices (Fig. 1). The vortex-induced normal force and pitching moment characteristics were extracted from the experimental data by subtracting from the measured C_N and C_m values the slender body normal force, computed as $C_N(\alpha) = C_{N\alpha}(O) \sin \alpha \cos \alpha$

cos ($\alpha/2$)(adapting the method of Refs. 23 and 24 for both the normal force and the corresponding moment).

Computed centers of pressure lie somewhat aft of the experimental values for both the vortex-induced normal force and side force (Figs. 9 and 10). Repeat runs and comparisons between different tests indicate the data accuracy for the center of pressure to be approximately $\Delta x_{CP}/d = 0.3$. Even in view of that, however, there is a persistent trend for the measurements to be forward of the predictions. Why?

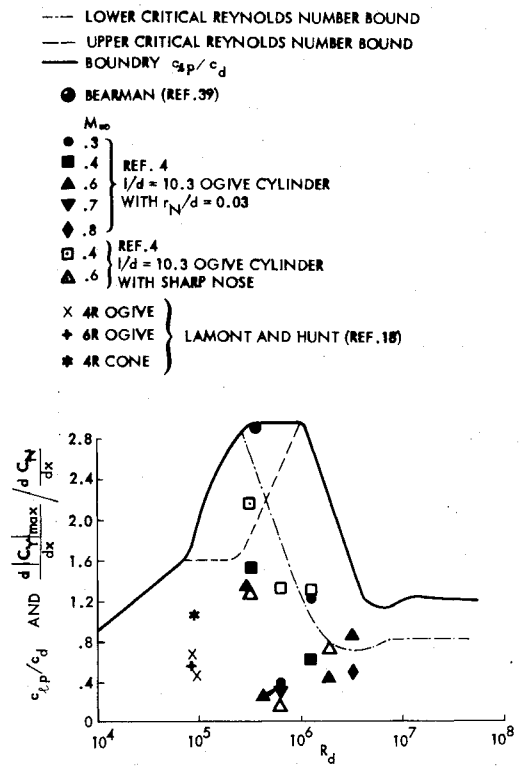

Fig. 7 Comparison of section lift/drag ratio on a cylinder in crossflow with the peak sectional side force/normal force ratio on a slender body.

Leading edge vortices on delta wings depart before the trailing edge due to the influence of the wake, thereby losing lift-generating power. The data obtained by Keener et al.[9] on a pointed ogive with and without the downstream presence of a cylindrical afterbody indicate that the wake causes a similar loss of the vortex-induced normal force on bodies of revolution. Assuming that the forward shift of the center of pressure is the same as for the delta wing, the method of Refs. 44 and 45 has been used to compute the results shown in Figs. 9 and 10. It can be seen that the match between predicted and measured centers of pressure has improved. Assuming that the side force has the same forward shift of the center of pressure improves the match between predictions and experiment for the side force. A forward movement of the center of pressure both for normal force and side force is documented by the measurements with and without a cylindrical aftbody performed by Keener et al.[9]

Secondary Vortex Effects

The supercritical boundary in Fig. 8 is shown as a phantom line because secondary vortices could alter this boundary due to critical Reynolds number effects. Evidence of the existence of secondary vortices is present in Fig. 1 as secondary suction peaks in the pressure distributions. The secondary vortex moves outboard until its suction peak cannot be distinguished from the attached flow suction peak near the lateral meridian. The position of the secondary vortices is governed by the Reynolds number of the secondary flow, which develops on the leeside of the slender body as the result of freestream air entrainment through the action of the primary vortices. When transition occurs in the secondary flow (before rollup),[46] the secondary vortex will move outboard. Similar effects occur on a delta wing.[47]

It is easy to see how asymmetries in the secondary vortices can result in an additional vortex-induced side force. Asymmetric transition in the secondary flow can cause one of the secondary vortex-induced suction peaks to move around to the side of the body, contributing to the vortex-induced side force. This side force component will persist until the transition becomes symmetric and the opposite secondary vortex also moves to the lateral meridian. Thus, the $|C_Y|_{max}/C_N$ bounds could be altered in the supercritical flow region by critical Reynolds number effects in the secondary flow. It is

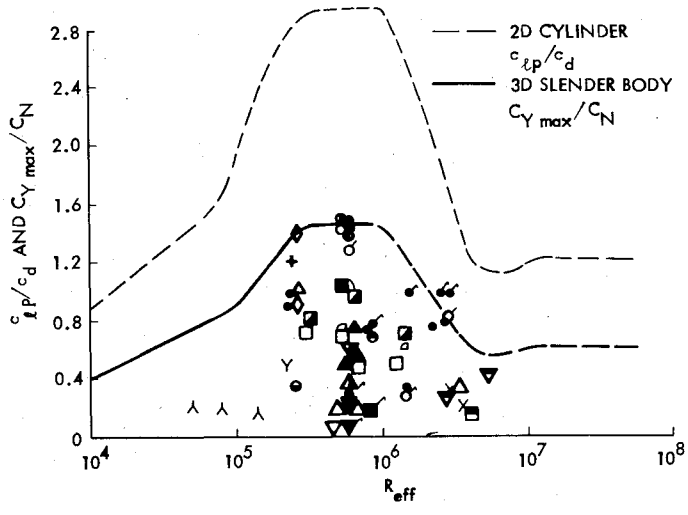

SYMBOL	REF	M_∞	CONFIG	ℓ/d
◐	42	0.25	OGIVE	3.5
○	9	0.25	OGIVE	3.5
□	9	0.6	OGIVE	3.5
△	9	0.8	OGIVE	3.5
▽	9	0.9	OGIVE	3.5
◇	2	LOW SUBSONIC	OGIVE	3.5
◇	2	LOW SUBSONIC	OGIVE	3.5
●	4	0.25	OGIVE	3.5
■	4	0.4	OGIVE	3.5
▲	4	0.6	OGIVE	3.5
▼	4	0.7	OGIVE	3.5
◑	9	0.25	OGIVE	5.0
◪	9	0.6	OGIVE	5.0
◬	9	0.8	OGIVE	5.0
▽	9	0.9	OGIVE	5.0
◢	4	0.25	OGIVE-CYL	7.0
◢	4	0.42	OGIVE-CYL	7.0
◢	4	0.62	OGIVE-CYL	7.0
◢	4	0.72	OGIVE-CYL	7.0
+	2	0.25	CONE	16°
◒	2	LOW SUBSONIC	PARABOLID	3.5
◒	1	0.57	OGIVE-CYL	8.18
◧	43	0.6	OGIVE-CYL	15
◆	43		OGIVE-CYL	11
X	13	0.5	OGIVE-CYL	17
■	13		CONE-CYL	17
▷	9	0.25	CONE-CYL	11
▷	9	0.6	CONE	20°
▷	9	0.8	CONE	20°
◶	4	0.25	OGIVE-CYL DETACHED	3.5(7)
Y	3	0.6	OGIVE-CYL	14.5
⅄	41	LOW SUBSONIC	OGIVE-CYL	15.0

Fig. 8 Maximum side force/normal force ratio.

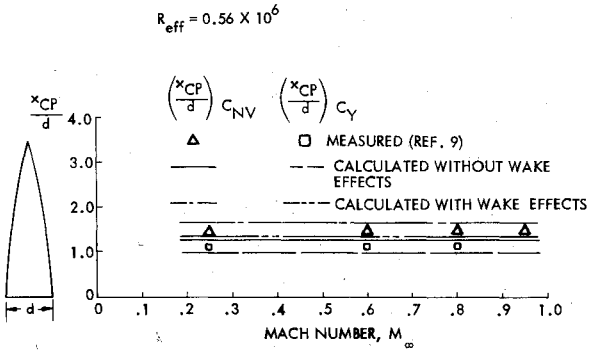

Fig. 9 Effect of Mach number on the centers of pressure of the vortex-induced loads on a 3.5 l/d tangent ogive when $|C_Y|$ is maximum.

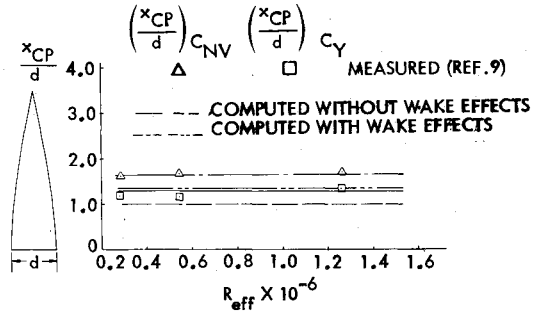

Fig. 10 Effect of Reynolds number on the center of pressure of the vortex-induced loads on a 3.5 l/d tangent ogive at $M_\infty = 0.6$ when $|C_Y|$ is maximum.

unfortunate that very little data are available for supercritical Reynolds numbers, which are of most practical interest. Such data could give valuable insight into the seriousness of these secondary flow effects.

Coupling with Body Motion

The literature contains some striking examples of coupling between vehicle motion and vortex shedding. Body spin,[48] coning,[49] and pitching motion[41] all affect the vortex shedding. Coupling effects will be especially large when boundary layer transition is involved since the vortex-induced side loads reach their maximum in this critical flow regime. The transition process itself is strongly coupled to vehicle motion (e.g., as in incompressible airfoil dynamics,[47] shock-boundary layer interaction at transonic speeds[50,51] or re-entry body dynamics at hypersonic speeds[52-54]).

Bearman's "frozen" subcritical-supercritical separation, which produced the maximum sectional out-of-plane load on a cylinder (Fig. 8),[39] is an example of the very large loads that could occur as the result of vehicle motion. At a specific critical Reynolds number Bearman found that the laminar bubble collapsed on one side only, producing the subcritical-supercritical separation.[39] The so-called leading edge jet effect, which is responsible for the large overshoot of $c_{l\max}$ for a pitching airfoil, can eliminate the laminar separation bubble on an airfoil[55] as is confirmed by recent experiments.[56] Similar effects can occur on the pitching and/or yawing missile body, eliminating the laminar bubble. Thus, the fact that body motion can lock in the maximum vortex-induced side force underscores the need for the control system to be capable of dealing with the maximum possible vortex-induced side force, which usually cannot be obtained by means other than those presented herein.

Conclusions

A method has been presented which successfully bounds the maximum vortex-induced side force and its accompanying yawing moment for incompressible speeds (where the side force is the greatest), over an effective Reynolds number range of 10^4 to 10^8. The method relates the maximum steady vortex-induced side force/normal force ratio on an inclined slender body of revolution to the maximum unsteady lift/drag ratio on a cylinder normal to the flow. This is accomplished through the use of an effective Reynolds number. The normalization of the maximum side force by the normal force facilitates the estimation of the maximum side force for a variety of body lengths, geometries, and angles of attack. Available evidence indicates that body motion could lock in the worst possible vortex asymmetry. Thus, the control system design must be capable of dealing with the maximum vortex-induced side force and yawing moment which at present cannot readily be determined by means other than the present technique. Although the present technique applies only to bodies dominated by a single asymmetric vortex pair, it could be extended to bodies dominated by multiple vortex pairs.

Acknowledgments

This paper is based upon results obtained in a study for the Naval Surface Weapons Center, Silver Spring, Md. (Contract N60921-77C-0234) under the direction of L.H. Schindel.

References

[1] Brown, R.C., "On the Asymmetrical Aerodynamic Forces of Slender Bodies of Revolution," *Proceedings of BOWACA Meeting,* McDonnell Aircraft Corp. St. Louis, Mo., 1965.

[2] Coe, P.L., Jr., Chambers, J.R., and Letko, W., "Asymmetric Lateral-Directional Characteristics of Pointed Bodies of Revolution at High Angles of Attack," NASA TN D-7095, Nov. 1972.

[3] Pick, G.S., "Investigation of Side Forces on Ogive-Cylinder Bodies at High Angles of Attack in the $M = 0.5$ to 1.1 Range," AIAA Paper 71-750, AIAA Fourth Fluid and Plasma Dynamics Conference, Palo Alto, Calif., June 21-23, 1971.

[4] Keener, E.R., Chapman, G.T., Cohen, L., and Taleghani, J., "Side Forces on a Tangent Ogive Forebody with a Fineness Ratio of 3.5 at High Angles of Attack and Mach Numbers from 0.1 to 0.7," NASA TM X-3437, Feb. 1977.

[5] Clark, W.H. and Peoples, J.R., "Occurrence and Inhibition of Large Yawing Moments During High-Incidence Flight of Slender Missile Configurations," *Journal of Spacecraft and Rockets,* Vol. 10, Aug. 1973, pp. 510-519.

[6] Thomson, K.D. and Morrison, D.F., "The Spacing, Position and Strength of Vortices in the Wake of Slender Cylindrical Bodies at Large Incidence," *Journal of Fluid Mechanics*, Vol. 50, Part 4, Dec. 1977, pp. 751-783.

[7] Reding, J.P. and Ericsson, L.E., "Maximum Vortex-Induced Side Force," *Journal of Spacecraft and Rockets,* Vol. 15, July-Aug. 1978, pp. 201-207.

[8] Nelson, R.C. and Fleeman, E.L., "High Angle-of-Attack Aerodynamics on a Slender Body with a Jet Plume," *Journal of Spacecraft and Rockets,* Vol. 12, Jan. 1975, pp. 12-16.

[9] Keener, E.R. and Taleghani, J., "Wind Tunnel Investigation of Aerodynamic Characteristics of Five Forebody Models at High Angles of Attack at Mach Numbers from 0.25 to 2," NASA TM X-73, 076, Dec. 1975.

[10] Dalhem, V. and Shereden, D., private communications of unpublished wind tunnel data, Flight Dynamics Laboratory, Wright-Patterson Air Force Base, Ohio, May 2, 1978 and Aug. 20, 1978.

[11] Dalhem, V., "Semi-Empirical Prediction Method for Induced Side Forces on Missiles at High Angles of Attack," Paper 38, 11th Navy Symposium on Aeroballistics, NADC, Warminister, Pa., Aug. 1979.

[12] Hoerner, S.F., *Fluid Dynamic Drag.* Hoerner Fluid Dynamics, Brick Town, N.J., 1958.

[13] Atraghji, E.G., "The Influence of Mach Number, Reynolds Number, Semi-Nose Angle, and Roll Rate on the Development of the Forces and Moments Over a Series of Long Slender Bodies of Revolution at Incidence," National Research Council, Ottawa, Canada, NAE High Speed Aerodynamics Section Rept. 545/0020, Sept. 6, 1967.

[14] Clarkson, M.H., Malcolm, G.N., and Chapman, G.T., "A Subsonic, High Angle of Attack Flow Investigation at Several Reynolds Numbers," *AIAA Journal*, Vol. 16, No. 1, June 1978, pp. 53-60.

[15] Bursnall, W.J. and Loftin, L.K., Jr., "Experimental Investigation of the Pressure Distribution about a Circular Cylinder in the Critical Reynolds Number Range," NACA TN 2463, Sept. 1951.

[16] Ericsson, L.E. and Reding, J.P., "Vortex-Induced Asymmetric Loads on Slender Vehicles," Lockheed Missiles & Space Co., Inc., Sunnyvale, Calif., LMSC-D630807, Jan. 1979.

[17] Clark, W.H., "Body Vortex Formation on Missiles in Incompressible Flows," AIAA Paper No. 77-1154, Aug. 1977.

[18] Lamont, P.J. and Hunt, B.L., "Pressure and Force Distributions on a Sharp-Nosed Cylinder at Large Angles of Inclination to a Uniform Subsonic Stream," *Journal of Fluid Mechanics,* Vol. 76, Part 3, Aug. 1976, pp. 519-559.

[19] Sarpkaya, T., "Separated Flow About Lifting Bodies and Impulsive Flow About Cylinders," *AIAA Journal*, Vol. 4, March 1966, pp. 414-426.

[20] Ericsson, L.E. and Reding, J.P., "Dynamic Stall Analysis in Light of Recent Numerical and Experimental Results," *Journal of Aircraft*, Vol. 13, April 1976, pp. 248-255.

[21] Ericsson, L.E. and Reding, J.P., "Spilled Leading Edge Vortex Effects on Dynamic Stall," *Journal of Aircraft,* Vol. 13, June 1977, pp. 313-315.

[22] Ericsson, L.E. and Reding, J.P., "Further Consideration of Spilled Leading Edge Vortex Effects on Dynamic Stall," *Journal of Aircraft*, Vol. 14, June 1977, pp. 601-603.

[23] Allen, H.J. and Perkins, E.W., "Characteristics of Flow over Inclined Bodies of Revolution," NACA RM A50 L07, 1951.

[24] Jorgensen, L.H., "Prediction of Static Aerodynamic Characteristics for Space Shuttle-Like and Other Bodies at Angles of Attack from 0° to 180°," NASA TN D-6996, June 1973.

[25] Loiseau, H. and Szechenui, E., "Analyse Experimental des Portances sur un Cylindre Immobile Soumis a un Ecoulement Perpendiculaire a son Axe a des Nombres de Reynolds Elevés," *La Recherche Aérospatiale,* Sept.-Oct. 1972, pp. 279-291.

[26] Humphreys, J.S., "On a Circular Cylinder in a Steady Wind at Transition Reynolds Numbers," *Journal of Fluid Mechanics*, Vol. 9, Part 4, 1960, pp. 603-612.

[27] Fung, Y.C., "Fluctuating Lift and Drag Acting on a Cylinder in a Flow at Supercritical Reynolds Numbers," *Journal of the Aeronautical Sciences,* Vol. 27, Nov. 1960, pp. 801-814.

[28] Van Nunen, J.W.G., Persoon, A.J., and Tijdeman, H., "Analysis of Steady and Unsteady Pressure and Force Measurements on a Circular Cylinder at Reynolds Numbers up to 7.7×10^6, NLR, The Netherlands, NLR TR 69102 U, May 1971.

[29] Schlinker, R.W., Fink, M.R., and Amiet, R.K., "Vortex Noise From Non-Rotating Cylinders and Airfoils," AIAA Paper No. 76-81, Jan. 1976.

[30] Gerrard, J.W., "An Experimental Investigation of the Oscillatory Lift and Drag of a Circular Cylinder Shedding Turbulent Vortices," *Journal of Fluid Mechanics*, Vol. 11, Part 2, Sept. 1961, pp. 244-256.

[31] Keefe, R.T., "An Investigation of the Fluctuating Forces Acting on a Stationary Circular Cylinder in a Subsonic Stream and of the Associated Sound Field," University of Toronto, Report UTIA No. 76, Sept. 1961.

[32] Goldman, R.L., "Karman Vortex Forces on a Vanguard Rocket," *Shock and Vibration Bulletin,* Part 11, Naval Research Laboratory, Washington, D.C., 1958.

[33] McGregor, D.M., "An Experimental Investigation of the Oscillatory Pressures on a Circular Cylinder in a Fluid Stream," University of Toronto, Institute of Aerophysics, Technical Note 14, 1957.

[34] Batham, J.P., "Pressure Distributions on Circular Cylinders of Critical Reynolds Number," *Journal of Fluid Mechanics*, Vol. 57, 1973, pp. 209-228.

[35] Kacker, S.C., Pennington, B., and Hill, R.S., "Fluctuating Lift Coefficient for a Circular Cylinder in Cross Flow," *Journal of Mechanical Engineering Sciences*, Vol. 16, No. 9, 1974, pp. 215-224.

[36] Schmidt, L.V., "Measurement of Fluctuating Air Loads on a Circular Cylinder," *Journal of Aircraft*, Vol. 2, Jan. 1965, pp. 49-55.

[37] Schmidt, L.V., "Fluctuating Force Measurements Upon a Circular Cylinder at Reynolds Numbers up to 5×10^6," Paper No. 19, Meeting on Ground Wind Load Problems in Relation to Launch Vehicles, NASA TM X-57779, 1966.

[38] Jones, G.W., Jr., "Unsteady Lift Forces Generated by Vortex Shedding About a Large, Stationary, and Oscillating Cylinder at High Reynolds Numbers," presented at the ASME Symposium on Unsteady Flow at the Fluids Engineering Conference, Philadelphia, Pa., May 6-9, 1968.

[39] Bearman, P.W., "On Vortex Shedding from a Circular Cylinder in the Critical Reynolds Number Regime," *Journal of Fluid Mechanics*, Vol. 37, Part 3, 1969, pp. 577-585.

[40] Wardlaw, A.B. and Morrison, A.M., "Induced Side Forces at High Angles of Attack," NSWC/WOL/TR 75-16, Nov. 1975.

[41] Smith, L.H., "Aerodynamic Characteristics of an Axisymmetric Body Undergoing a Uniform Pitching Motion," Ph.D. Thesis, Naval Postgraduate School, Monterey, Calif., Dec. 1974.

[42] Keener, E.R., Chapman, G.T., and Kruse, R.L., "Effects of Mach Number and Afterbody Length on Onset of Asymmetric Forces on Bodies at Zero Side Slip and High Angles of Attack," AIAA Paper 76-66, AIAA 14th Aerospace Sciences Meeting, Washington, D.C., June 26-28, 1976.

[43] Kubin, J.S., "An Analysis of Steady Asymmetric Vortex Shedding from a Missile at High Angle of Attack," Air Force Institute of Technology, AD-774390, Nov. 1973.

[44] Ericsson, L.E. and Reding, J.P., "Approximate Nonlinear Slender Wing Aerodynamics," *Journal of Aircraft*, Vol. 14, Dec. 1977, pp. 1197-1204.

[45] Ericsson, L.E. and Reding, J.P., "Unsteady Aerodynamic Analysis of Space Shuttle Vehicles, Part II, Steady and Unsteady Aerodynamics of Sharp-Edged Delta Wings," NASA CR-124423, Aug. 1973.

[46] Hummel, D., "Experimentelle Untersuchung der Strömung auf der Saugseite eines Schlanken Delta Flügels," *Zeitschrift für Flugwissenschaften*, Vol. 13, July 1965, pp. 247-252.

[47] Ericsson, L.E. and Reding, J.P., "Dynamic Stall of Helicopter Blades," *Journal of American Helicopter Society*, Vol. 17, Jan. 1972, pp. 10-19.

[48] Kruse, R.L., "Influence of Spin Rate on Side Force of an Axisymmetric Body," *AIAA Journal*, Vol. 16, April 1978, pp. 415-416.

[49] Schiff, L.B. and Tobak, M., "Results from a New Wind Tunnel Apparatus for Studying Coning and Spinning Motions of Bodies of Revolution," *AIAA Journal*, Vol. 8, Nov. 1970, pp. 1953-1958.

[50] Ericsson, L.E. and Reding, J.P., "Scaling Problems in Dynamic Tests of Aircraft-Like Configurations," Paper 25, AGARD CP-227, AGARD Conference on Unsteady Aerodynamics, Ottawa, Canada, Sept. 26-28, 1973.

[51] Ericsson, L.E., "Dynamic Effects of Shock-Induced Flow Separation," *Journal of Aircraft*, Vol. 12, Feb. 1975, pp. 86-92.

[52] Ericsson, L.E., "Effects of Boundary Layer Transition on Vehicle Dynamics," *Journal of Spacecraft and Rockets,* Vol. 6, Dec. 1969, pp. 1404-1409.

[53] Ericsson, L.E., "Transition Effects on Stability and Trim Characteristics," *Journal of Spacecraft and Rockets,* Vol. 11, Jan. 1974, pp. 3-11.

[54] Ericsson, L.E., "Correlation of Attitude Effects on Slender Vehicle Transition," *AIAA Journal*, Vol. 12, April 1974, pp. 523-529.

[55] Ericsson, L.E. and Reding, J.P., "Analytic Prediction of Dynamic Stall Characteristics," AIAA Paper No. 72-682, June 1972.

[56] Carr, L.W., McAllister, K.W., and McCroskey, W.J., "Analysis of the Development of Dynamic Stall Based on Oscillating Experiments," NASA TN D-8382, June 1977.